THE ASTROPHYSICAL JOURNAL, 436:L67–L70, 1994 November 20


# TEMPERATURE AND IRON ABUNDANCE VARIATION OF THE GAS IN THE PERSEUS CLUSTER

K. A. ARNAUD[1] AND R. F. MUSHOTZKY
Laboratory for High Energy Astrophysics, NASA/GSFC, Greenbelt MD 20771
H. EZAWA AND Y. FUKAZAWA
Department of Physics, University of Tokyo, Bunkyo-ku, Tokyo 113, Japan
T. OHASHI
Department of Physics, Tokyo Metropolitan University, Hachioji, Tokyo 192-03, Japan
M. W. BAUTZ, G. B. CREWE, AND K. C. GENDREAU
Center for Space Research, Massachusetts Institute of Technology, Cambridge, MA 02139
AND
K. YAMASHITA, Y. KAMATA, AND F. AKIMOTO
Department of Astrophysics, Nagoya University, Chikusa-ku, Nagoya 464-01, Japan
*Received 1994 June 6; accepted 1994 August 26*

## ABSTRACT

We present the first two-dimensional map of the temperature and iron abundance in the Perseus cluster. Analysis of spectra obtained using the Gas Imaging Spectrometer on *ASCA* shows nonaxisymmetric variations in both the temperature and iron abundance. Traveling west from the cluster center, the temperature increases to 9 keV at 20′ and then decreases rapidly to 5 keV at 40′. There is a hot (>10 keV) region to the northwest of the cluster center. The abundance is approximately constant over much of the surveyed region, but there is evidence for an increased abundance in the northwest hot area and a gradual decrease in a westerly direction.

*Subject headings:* galaxies: clusters of

## 1. INTRODUCTION

The Perseus cluster is one of the brightest, best observed, extragalactic X-ray sources. Low-resolution (20%) spectroscopy using wide-field collimated detectors established that the emission from the Perseus cluster is due to thermal bremsstrahlung and line emission in a hot plasma (Serlemitsos et al. 1977; Mitchell et al. 1976). The confirming evidence for this hypothesis was the detection of the Fe-K$\alpha$ line at $\sim$6.7 keV.

These early observations measured the emission-weighted mean temperature and iron abundance of the gas component of the Perseus cluster. Useful as these measurements are, spatially resolved temperatures and abundances are required to determine the hydrodynamic and thermodynamic structures of the gas. Spatially resolved gas temperatures can be used to map the total gravitating matter content of the cluster and hence the size and structure of the dark matter component (Fabricant & Gorenstein 1983). Spatially resolved iron abundances provide important clues to the formation mechanism of the cluster and the source of the X-ray emitting gas (e.g., Kowalski et al. 1993; Metzler & Evrard 1994). For these reasons, spatially resolved spectroscopy of clusters has been one of the Holy Grails[2] of X-ray astronomy.

This *Letter* describes the first results from the observations of the Perseus cluster using the *Advanced Satellite for Cosmology and Astrophysics* (*ASCA*) (Tanaka, Inoue, & Holt 1994). Here we discuss the large-scale variations in temperature and abundance based on data from the Gas Imaging Spectrometer (GIS) (Kohmura et al. 1993). The central cooling flow is treated elsewhere (Fabian et al. 1994). We will consider the surface brightness distribution and data from the other detectors on *ASCA* in a later paper.

## 2. DATA ANALYSIS AND RESULTS

*ASCA* performed three observations of the Perseus cluster in 1994 June as part of the performance verification phase. The three pointings were designed to map the center of the cluster and to extend west to IC 310. The fields covered by the GIS (Kohmura et al. 1993) have a considerable overlap and enable us to compare spectra of identical regions of the cluster which appear on different parts of the detector. The observation details are summarized in Table 1.

We extracted clean X-ray event lists for GIS2 and GIS3 by using a cutoff rigidity threshold of eight and standard techniques to reject background contamination. We generated spectra by laying down a grid of 8′ by 8′ squares, centered on NGC 1275 and oriented east-west–north-south. The events in each square for each GIS and observation were extracted to give a number of spectra for each position in the cluster. The instrument response for each square was created from a count-weighted sum of responses over the instrument pixels contained in the square. A background spectrum for each source spectrum was made by extracting events from the summed blank fields provided by the *ASCA* Guest Observer Facility. These events were filtered identically to the Perseus observations and then extracted from an identical region on the detector used for each source spectrum.

We determined temperatures and iron abundances for each square in the grid by simultaneously fitting all spectra for that grid square to a model consisting of an isothermal Raymond-

[1] Also Astronomy Department, University of Maryland.
[2] In view of the frequent use of the Holy Grail metaphor, it is worth recalling that the person who found it was he who sat in the Siege Perilous.

TABLE 1

OBSERVATION DETAILS

| Number | Detector | R.A.[a] | Declination[a] | Roll | Time[b] |
|---|---|---|---|---|---|
| 1..... | GIS2 | 50.0336 | 41.6391 | −79.72 | 15145 |
| 1..... | GIS3 | 50.0363 | 41.6143 | −79.72 | 15144 |
| 2..... | GIS2 | 49.6299 | 41.5348 | −79.23 | 17859 |
| 2..... | GIS3 | 49.6328 | 41.5100 | −79.23 | 17857 |
| 3..... | GIS2 | 49.2788 | 41.5498 | −59.94 | 21481 |
| 3..... | GIS3 | 49.2924 | 41.5271 | −59.94 | 19405 |

[a] J2000.

[b] Net time (in seconds) after rejection of high background intervals.

Smith plasma model (Raymond & Smith 1977 and improvements) modified by photoelectric absorption. The simultaneous fit forced each spectrum in a given grid square to have the same temperature, abundance, and absorption column, but the normalizations were allowed to vary between spectra. Figure 1 shows three example spectra and best-fit models. Table 2 summarizes the results of these fits. The uncertainty ranges given are 90% confidence for one interesting parameter ($\Delta\chi^2 + 2.71$). The Raymond-Smith model which was fitted uses heavy element abundance ratios from Anders & Grevesse (1989). In practice, the measured abundance is dominated by that of iron.

Most grid squares had more than one spectrum, so we are able to check our results by comparing temperatures for the same part of the cluster observed by different detectors and by different parts of the same detector. We find no systematic differences between temperatures determined from GIS2 and GIS3 and no systematic differences when comparing spectra from the same sky region taken at different positions on the detector.

We have plotted two different representations of our results. Figure 2 shows two-dimensional representations of the temperature and abundance, and Figure 3 shows these quantities along cuts through the cluster center in the east-west and

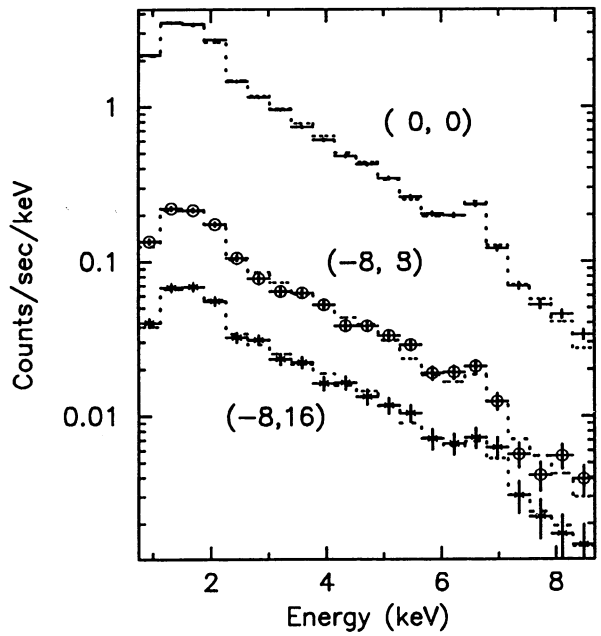


FIG. 1.—Example spectra and best-fit models. The pairs of numbers for each spectrum refer to the offsets in Table 2.

TABLE 2

RESULTS

| Offset[a] (R.A., decl.) | $\chi^2/N$ | $N$ | Temperature[b] | Abundance[c] |
|---|---|---|---|---|
| −8, −16 | 0.89 | 17 | $14.23^{+13.7}_{-4.99}$ | $0.61^{+0.69}_{-0.60}$ |
| −16, −16 | 0.77 | 38 | $9.59^{+3.85}_{-2.26}$ | $0.46^{+0.31}_{-0.28}$ |
| −24, −16 | 1.16 | 59 | $7.06^{+2.69}_{-1.66}$ | $0.20^{+0.28}_{-0.20}$ |
| −32, −16 | 1.30 | 38 | $5.16^{+1.63}_{-1.10}$ | $0.21^{+0.35}_{-0.21}$ |
| 16, −8 | 1.43 | 17 | $7.54^{+2.05}_{-1.50}$ | $0.50^{+0.28}_{-0.25}$ |
| 8, −8 | 1.12 | 38 | $8.67^{+1.03}_{-0.95}$ | $0.47^{+0.12}_{-0.11}$ |
| 0, −8 | 1.43 | 59 | $7.75^{+0.61}_{-0.52}$ | $0.44^{+0.07}_{-0.07}$ |
| −8, −8 | 1.24 | 59 | $8.92^{+0.93}_{-0.79}$ | $0.48^{+0.09}_{-0.10}$ |
| −16, −8 | 1.26 | 80 | $8.78^{+1.17}_{-1.02}$ | $0.32^{+0.12}_{-0.11}$ |
| −24, −8 | 1.20 | 80 | $10.11^{+2.03}_{-1.52}$ | $0.29^{+0.16}_{-0.16}$ |
| −32, −8 | 1.07 | 59 | $5.72^{+1.24}_{-0.88}$ | $0.23^{+0.18}_{-0.17}$ |
| −40, −8 | 0.91 | 38 | $5.29^{+1.82}_{-1.28}$ | <0.28 |
| 16, 0 | 2.18 | 38 | $7.28^{+0.91}_{-0.70}$ | $0.55^{+0.12}_{-0.12}$ |
| 8, 0 | 1.31 | 38 | $6.36^{+0.31}_{-0.30}$ | $0.35^{+0.05}_{-0.04}$ |
| 0, 0 | 4.65 | 80 | $4.56^{+0.06}_{-0.07}$ | $0.38^{+0.02}_{-0.02}$ |
| −8, 0 | 1.38 | 80 | $6.65^{+0.29}_{-0.28}$ | $0.37^{+0.05}_{-0.04}$ |
| −16, 0 | 1.59 | 80 | $8.84^{+0.85}_{-0.78}$ | $0.32^{+0.08}_{-0.09}$ |
| −24, 0 | 1.27 | 80 | $9.61^{+1.62}_{-1.10}$ | $0.27^{+0.13}_{-0.12}$ |
| −32, 0 | 1.09 | 59 | $5.84^{+1.14}_{-0.86}$ | $0.17^{+0.16}_{-0.15}$ |
| −40, 0 | 1.79 | 38 | $5.41^{+1.96}_{-1.24}$ | $0.22^{+0.36}_{-0.22}$ |
| 16, 8 | 0.55 | 17 | $7.70^{+1.63}_{-1.19}$ | $0.59^{+0.20}_{-0.19}$ |
| 8, 8 | 0.98 | 38 | $6.99^{+0.45}_{-0.43}$ | $0.33^{+0.06}_{-0.06}$ |
| 0, 8 | 1.45 | 80 | $6.47^{+0.30}_{-0.29}$ | $0.37^{+0.04}_{-0.05}$ |
| −8, 8 | 1.76 | 80 | $9.43^{+0.96}_{-0.68}$ | $0.49^{+0.08}_{-0.09}$ |
| −16, 8 | 1.30 | 80 | $11.95^{+2.60}_{-1.47}$ | $0.69^{+0.18}_{-0.17}$ |
| −24, 8 | 1.09 | 80 | $10.63^{+2.45}_{-1.74}$ | $0.33^{+0.17}_{-0.18}$ |
| −32, 8 | 0.89 | 80 | $8.28^{+2.16}_{-1.69}$ | <0.17 |
| −40, 8 | 0.60 | 17 | $4.05^{+2.53}_{-1.34}$ | $0.08^{+0.57}_{-0.08}$ |
| 16, 16 | 1.30 | 38 | $7.80^{+2.36}_{-1.55}$ | $0.48^{+0.25}_{-0.25}$ |
| 8, 16 | 1.08 | 38 | $8.27^{+1.48}_{-1.24}$ | $0.50^{+0.16}_{-0.16}$ |
| 0, 16 | 0.79 | 59 | $11.36^{+2.67}_{-1.88}$ | $0.72^{+0.24}_{-0.21}$ |
| −8, 16 | 0.88 | 80 | $17.05^{+6.70}_{-4.39}$ | $0.88^{+0.41}_{-0.33}$ |
| −16, 16 | 1.31 | 38 | $14.31^{+10.2}_{-4.43}$ | $0.88^{+0.76}_{-0.53}$ |
| −24, 16 | 1.03 | 80 | $6.00^{+1.93}_{-1.17}$ | $0.66^{+0.36}_{-0.29}$ |
| −32, 16 | 0.88 | 38 | $4.87^{+2.20}_{-1.20}$ | $0.29^{+0.44}_{-0.29}$ |
| −40, 16 | 1.52 | 17 | $2.55^{+2.91}_{-1.13}$ | <1.69 |

[a] Offset from NGC 1275 in arcminutes. The first column is right ascension and the second declination.

[b] Temperature in keV. The errors given are 90% confidence.

[c] Iron abundance relative to Fe/H = $4.68 \times 10^{-5}$. The errors given are 90% confidence.

north-south directions. A number of features of these plots stand out. The grid square centered on NGC 1275 is at a temperature minimum and is very poorly fitted by a single-temperature model. This is not a new result, although these data are far better than any available previously and the detailed analysis does show new features (Fabian et al. 1994). Ignoring this central bin, there is very strong evidence for a variation in temperature and abundance. Fitting all the temperatures to a single value gives a reduced $\chi^2$ of 7, and doing the same for the abundances gives a reduced $\chi^2$ of 3.5.

In the westerly direction there is a temperature maximum of 8–10 keV at 20′–25′ from NGC 1275 and then a sharp decrease back to less than 6 keV. East from the center the temperature also rises but not as steeply as to the west, and our data do not

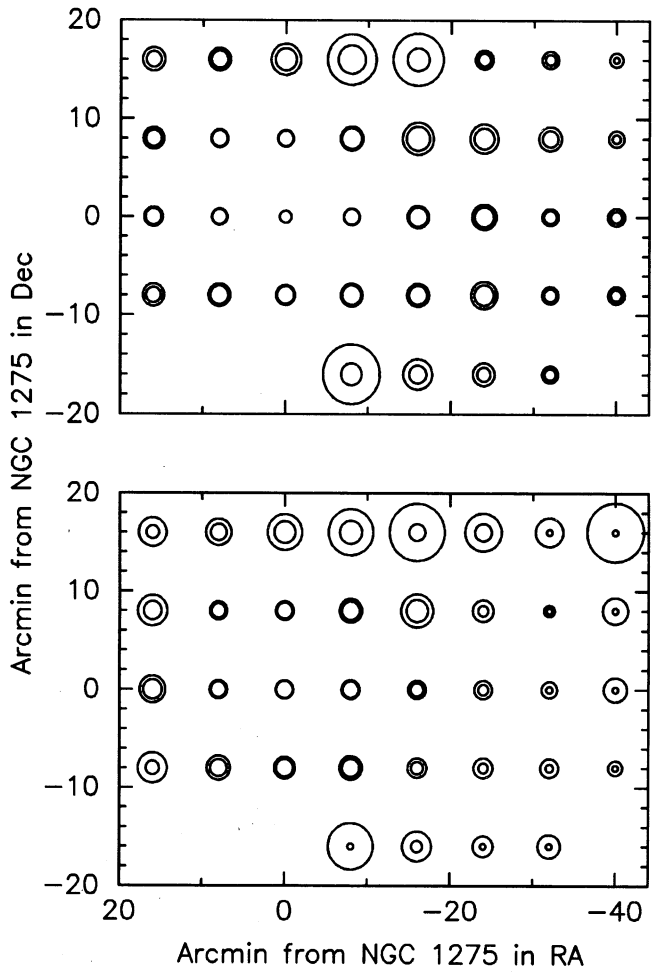


FIG. 2.—Representations of the (*top*) temperature and (*bottom*) abundance variations in the Perseus cluster. The radii of the circles are proportional to the quantity being mapped, the inner circle being the low end and the outer circle being the high end of the 90% confidence range.

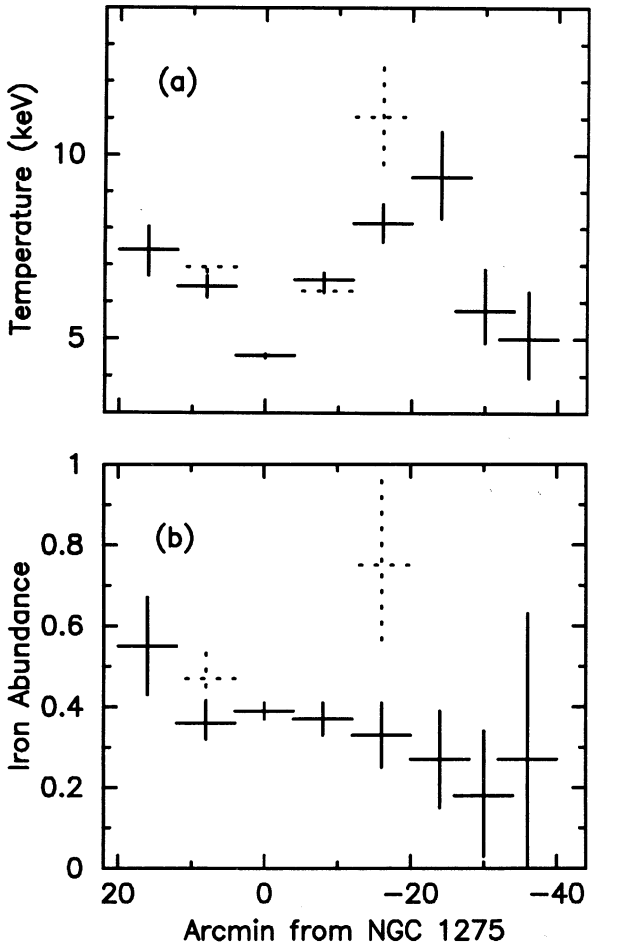


FIG. 3.—Profiles of (*a*) temperature and (*b*) abundance variations through the cluster center. The solid crosses are an east-west slice, and the dashed crosses are north-south. The vertical bar gives the 90% confidence range, and the horizontal bar gives the size of the region from which the spectra were extracted.

extend far enough to see whether there is a temperature maximum. North west of the cluster center there is a sharp increase in temperature to more than 10 keV.

There is a gradual decrease in abundance to the west while the results to the east are more ambiguous. There appears to be an abundance enhancement to the northwest, but further observations are required to confirm this.

Eight of the grid squares have $\chi^2$ values that are unacceptable at the 5% level. We would expect two, so the isothermal model is probably not a complete description of the data (as we know to be the case for the grid square centered on NGC 1275).

## 3. DISCUSSION

### 3.1. *The Temperature Map*

Previous measurements of the emission-weighted gas temperature have given $\sim 6.5$ keV for the central 40′–1° (e.g., Allen et al. 1992). Eyles et al. (1991) fitted their coded aperture mask spectra with a variety of models for the radial variation in temperature. Their general result is that the temperature decreases with increasing radius but with a central cooling flow component that reduces the measured temperature in the central $\sim 5'$. The Spartan experiment found a similar result, a temperature within the central 5′ of 3.6 keV and then a profile almost isothermal from 6′–50′ with a temperature of 6.5 keV (Snyder et al. 1990; Kowalski et al. 1993). BBXRT found a low temperature in the center of the cluster with an increase to 8–10 keV by 15′ to the west (Arnaud et al. 1993). The *ASCA* results are broadly consistent with previous observations but show more detail. In particular, the hotter region to the northwest of the cluster center had not been suspected since the *ROSAT* image (Schwarz et al. 1992) shows no distinct features there. A temperature map of the whole cluster is required to tell whether this is an isolated feature or part of a larger pattern.

The observed distribution in temperatures is a considerable challenge to theoretical models. Because the cooling radius in the Perseus cluster is $\sim 5'$ (Arnaud 1986), not all the increase in temperature from 4.5 keV to $\sim 9$ keV over the central 20′ can be due to the cooling flow. The joint $N$-body and gas hydrodynamic simulation of Thomas & Couchman (1992) does show a temperature structure reminiscent of that seen in our data. These authors attribute this increase in temperature with radius to the fact that particles that end up in the central region of the cluster tend to have started there and have not obtained the full energy of the potential well. However, other simula-

tions (Metzler & Evrard 1994; Tsai et al. 1994) do not reproduce this result.

Another possibility is that the cluster is not in equilibrium, and the temperatures are not determined by hydrostatic balance. Theoretical modeling of high-velocity cluster mergers (Roettinger, Burns, & Loken 1993; Schindler & Muller 1993) shows that there can be significant temperature variations which are not accompanied by obvious X-ray emissivity changes. The spatial structure of the temperature variation shown in the Schindler & Muller (1993) paper, the only one of which we are aware with figures showing the X-ray temperature evolution during a merger, is in good qualitative agreement with our Perseus data if we assume that the merging component came from the east. However, the temperatures predicted are considerably higher than those seen with *ASCA* data, and it is difficult to understand why we should still see a cooling flow.

If a cluster such as Perseus, which has not been suspected of being a merger (but see Schwarz et al. 1992), has gas temperatures that are not determined solely by hydrostatic support, then considerable care must be taken in deducing dark matter profiles, especially for clusters that do not have the wealth of data available for Perseus.

### 3.2. *The Abundance Map*

The large field-of-view collimator experiments have established that the emission-weighted iron abundance over the central $\sim 1°$ is 0.27 solar (where solar is Fe/H $= 4.68 \times 10^{-5}$)[3] (e.g., Allen et al. 1992 and references therein). The distribution of iron within the cluster has been a source of controversy. Two experiments have found a strong decrease in the abundance with increasing radius (Ponman et al. 1990; Kowalski et al. 1993); one has found a central abundance consistent with the cluster mean (Mushotzky et al. 1981), and the most recent has found a constant abundance in the cluster core but with a value larger than the cluster mean (Arnaud et al. 1993).

The *ASCA* results show the presence of iron as much as 30′ (approximately 1 Mpc for $H_0 = 50$ km s$^{-1}$ Mpc$^{-1}$) to the West of the cluster center. This disagrees with the best-fit model of Kowalski et al. (1993) but is consistent with their range of acceptable models as represented in Figure 5*a* of that paper. We cannot make a statement about the abundance in the center of the cluster because we do not yet have a model that gives an adequate fit to the spectra from the central grid square.

The low-abundance region in the far west may be due to the group associated with IC 310. If so, this would be consistent with the low abundances seen in other low X-ray luminosity groups (Mulchaey et al. 1993). The high-abundance region is associated with the higher temperatures. If this region contains poorly thermalized gas, as predicted in the merger scenario, then the gas may be underionized because the timescale for electron-ion collisions can be significantly longer than that for electron-electron collisions. If the gas is underionized, then the line equivalent width for a given abundance will be higher, producing the result we see.

Metzler & Evrard (1994) have modeled the spatial distribution of heavy elements in an evolving cluster. They predict an abundance gradient and "patchiness" in the abundance. This occurs because the galaxies have a steeper radial profile than the intercluster gas, and enriched gas never moves far from the galaxy that produced it. While Perseus does not have the strong abundance gradient that *ASCA* has seen in some (but not most) clusters (Fukazawa et al. 1994), the patchiness is similar to that predicted by Metzler & Evrard (1994).

## 4. CONCLUSIONS

We have found nonaxisymmetric variations in temperature and abundance in the Perseus cluster. As expected, the cluster center is cooler than the mean; however, the temperature continues to rise with increasing radius outside the cooling region. There is a hot region to the northwest of the cluster center. The abundance decreases gradually to the west; however, there is iron observed as much as 1 Mpc from the cluster center. These observations provide important grist for the theorist's mills, and more extensive mapping of the Perseus cluster using *ASCA* will pay further dividends.

[3] This value (from Anders & Grevesse 1989) is higher than those usually used in X-ray astronomy, which are from long obsolete references from the 1970s.

## REFERENCES


Allen, S. W., Fabian, A. C., Johnstone, R. M., Nulsen, P. E. J., & Edge, A. C. 1992, MNRAS, 254, 51
Anders, E., & Grevesse, N. 1989, Geochim. Cosmochim. Acta, 53, 197
Arnaud, K. A. 1986, unpublished
Arnaud, K. A., et al. 1993, in Proc. *Ginga* Memorial Symp., ed. F. Makino & F. Nagase (Tokyo: ISAS), 114
Eyles, C. J., Watt, M. P., Bertram, D., Church, M. J., Ponman, T. J., Skinner, G. K., & Willmore, A. P. 1991, ApJ, 376, 23
Fabian, A. C., Arnaud, K. A., Bautz, M. W., & Tawara, Y. 1994, ApJ, 436, L63
Fabricant, D., & Gorenstein, P. 1983, ApJ, 267, 535
Fukazawa, Y., Ohashi, T., Fabian, A. C., Canizares, C. R., Ikebe, Y., Makishima, K., Mushotzky, R. F., & Yamashita, K. 1994, PASJ, 46, L55
Kowalski, M. P., Cruddace, R. G., Snyder, W. A., Fritz, G. G., Ulmer, M. P., & Fenimore, E. E. 1993, ApJ, 412, 489
Kohmura, Y., et al. 1993, Proc. SPIE, 2006, 78
Metzler, C., & Evrard, A. 1994, preprint
Mitchell, R. J., Culhane, J. L., Davison, P. J. N., & Ives, J. C. 1976, MNRAS, 176, 29P
Mulchaey, J., Davis, D., Mushotzky, R. F., & Burstein, D. 1993, ApJ, 404, L9
Mushotzky, R. F., Holt, S. S., Smith, B. W., Boldt, E. A., & Serlemitsos, P. J. 1981, ApJ, 244, L47
Ponman, T. J., Bertram, D., Church, M. J., Eyles, C. J., Watt, M. P., Skinner, G. K., & Willmore, A. P. 1990, Nature, 347, 450
Raymond, J. C., & Smith, B. W. 1977, ApJS, 35, 419
Roettinger, K., Burns, J., & Loken, C. 1993, ApJ, 407, 53
Schindler, S., & Muller, E. 1993, A&A, 272, 137
Schwarz, R. A., Edge, A. C., Voges, W., Boehringer, H., Ebeling, H., & Briel, U. G. 1992, A&A, 256, L11
Serlemitsos, P. J., Smith, B. W., Boldt, E. A., Holt, S. S., & Swank, J. H. 1977, ApJ, 211, L63
Snyder, W. A., Kowalski, M. P., Cruddace, R. G., Fritz, G. G., Middleditch, J., Fenimore, E. E., Ulmer, M. P., & Majewski, S. R. 1990, ApJ, 365, 460
Tanaka, Y., Inoue, H., & Holt, S. S. 1994, PASJ, 46, L37
Thomas, P. A., & Couchman, H. 1992, MNRAS, 257, 11
Tsai, J., Katz, N., & Bertschinger, E. 1994, ApJ, 423, 553